J|A|C|S
ARTICLES
Published on Web 08/15/2002

Exploring the Capabilities of X-ray Absorption Spectroscopy for Determining the Structure of Electrolyte Solutions: Computed Spectra for Cr^{3+} or Rh^{3+} in Water Based on Molecular Dynamics

Patrick J. Merkling,[†] Adela Muñoz-Páez,[‡] and Enrique Sánchez Marcos*,[†]

Contribution from the Departamento de Química Física and Departamento de Química Inorgánica-ICMSE, Universidad de Sevilla-CSIC, 41012 Sevilla, Spain

Received January 28, 2002

Abstract: Extended X-ray absorption fine structure (EXAFS) spectra of Cr^{3+} and Rh^{3+} in aqueous solution are analyzed and compared with computed spectra derived from structural results obtained by molecular dynamics (MD) simulation. This procedure quantifies the reliability of the EXAFS structural determination when applied to ions in solution. It provides guidelines for interpreting experimental spectra of octahedrally coordinated metal cations in aqueous solution. A set of relationships among Debye−Waller factors is proposed on the basis of MD results to reduce the number of independent fit parameters. The determination of the second hydration shell is examined. Calculated XANES spectra compare well with experimental ones. Indeed, the splitting observed on the main peak of the Rh K-edge was anticipated by the calculations. Simulated spectra from MD structures of increasing cluster size show a relationship between the second hydration shell and features of the XANES region at energies just above the edge. The combination of quantum and statistical calculations with the XANES spectrum is found to be very fruitful to get insight into the quantitative estimation of structural properties of electrolyte solutions.

Introduction

X-ray absorption spectroscopy (extended X-ray absorption fine structure, EXAFS, and X-ray absorption near-edge structure, XANES) has been used extensively in the past 25 years for extracting both qualitative and quantitative structural information around a moderately heavy atom. This technique is especially interesting in the case of dilute disordered systems.

In the EXAFS region of the spectrum, contributions from scattering paths to the total amplitude $\chi(k)$ as a function of the wave vector k can be expressed through the classical equation:[1,2]

$$\chi(k) = \sum_j \frac{N_j {S_0}^2}{k{R_j}^2} |f_j^{\mathrm{eff}}(k,R_j)| \sin(2kR_j + \varphi_j(k)) \times e^{-2R_j/\lambda(k)} e^{-2\sigma_j^2 k^2} \quad (1)$$

where the summation goes over all paths j. In this equation, N_j is the coordination number, ${S_0}^2$ the amplitude reduction factor, R_j the path length, f_j^{eff} the curved-wave backscattering amplitude, φ_j the phase-shift, λ the mean free path, and σ_j^2 the second-order cumulant known as the Debye−Waller (DW) factor. Theoretical advances have made it possible to obtain accurate theoretical values for the phase-shift, curved-wave backscattering amplitude, and mean free path for every scattered wave path by indicating or postulating the type of atoms involved.[3,4] If one dealt with the correct geometrical arrangement around the absorber atom, the structural problem would seem to reduce to a fitting procedure of distances and coordination numbers.

Unfortunately, the number of variables remaining is generally superior to the amount of information contained in the EXAFS spectrum.[2,5] Everyone working with EXAFS spectroscopy faces this problem. A series of assumptions has to be made a priori, e.g., a value for ${S_0}^2$, the paths to be considered and their distribution, etc. A strategy to help in the extraction of structural information contained in these spectra is to include independent information derived from computer simulations, which supplies us with a microscopic description of the close environment of the absorber atom. This procedure has been proven to be useful in the study of systems in solid and liquid states.[6−12]

* Address correspondence to this author. E-mail: sanchez@simulux.us.es.
[†] Departamento de Química Física.
[‡] Departamento de Química Inorgánica-ICMSE.

(1) Sayers, D. E.; Stern, E. A.; Lytle, F. W. *Phys. Rev. Lett.* **1971**, *27*, 1204.
(2) Koningsberger, D. C., Prins, R., Eds.; *X-ray Absorption: Principles, Applications, Techniques of EXAFS, SEXAFS, and XANES;* Wiley: New York, 1988.
(3) Rehr, J. J.; Albers, R. C. *Rev. Mod. Phys.* **2000**, *72*, 621.
(4) Joly, Y.; Cabaret, D.; Renevier, H.; Natoli, C. R. *Phys. Rev. Lett.* **1999**, *82*, 2398.
(5) Penner-Hahn, J. *Coord. Chem. Rev.* **1999**, *190−192*, 1101.
(6) Palmer, B. J.; Pfund, D. M.; Fulton, J. L. *J. Phys. Chem.* **1996**, *100*, 13393.
(7) Roccatano, D.; Berendsen, H. J. C.; D'Angelo, P. *J. Chem. Phys.* **1998**, *108*, 9487 and references therein.
(8) Filipponi, A.; D'Angelo, P.; Pavel, N. V.; Di Cicco, A. *Chem. Phys. Lett.* **1994**, *225*, 150.
(9) Spångberg, D.; Hermansson, K.; Lindqvist-Reis, P.; Jalilehvand, F.; Sandström, M.; Persson, I. *J. Phys. Chem. B* **2000**, *104*, 10467.

In contrast with EXAFS, in the XANES region not only scattering but also electronic phenomena play a major role. This has hampered the formulation of a simple equation that encompasses both aspects. This fact has led to the use of XANES on a more qualitative level, such as the identification of the symmetry environment of the absorber atom.[13] Nevertheless, the combination of quantum mechanical treatment of the phenomena reflected in the XANES region with the well-tested microscopic description of the close environment of the absorbing atom allows a more quantitative approach to the study of XANES spectra.[2,3,14]

The present work is framed within the ion solvation study of electrolyte aqueous solutions of transition metal cations. Several works, mainly dealing with divalent cations, have tackled this topic using MD simulations, focusing on the EXAFS part of the spectrum.[6,10,12] In the case of the trivalent metal cations chromium and rhodium, first-shell coordination number and octahedral geometry are well established.[15] Further, Cr^{3+} and Rh^{3+} are remarkable due to the extreme stability of their first hydration shell.[16] Therefore, since distortions in the first shell are expected to be small, an average structure representative of the trivalent cation plus its first hydration shell, called the hydrated ion, is the central entity. This solvation case seems especially suitable for a refined analysis of the structure beyond the first hydration shell. The use of such simple and well-defined systems allows an exploration of the XAS capabilities for metal cations in condensed phases.[17,18] The conclusions obtained may be extended to a variety of systems of practical interest, like metal centers in biochemical environments or metal catalysts.[5,19]

As a continuation of our experimental XAS studies on the Cr^{3+} hydration,[17,18,20] in two previous communications EXAFS[21] and XANES[22] spectra were computed with structural information derived from an MD simulation.[23] The satisfactory comparison between the computed and experimental spectra showed that the methodological procedure undertaken was appropriate. From it, several useful relationships among DW factors were observed, and an S_0^2 value was determined from comparison of computed and experimental EXAFS spectra. Rehr and colleagues[11] have also studied the EXAFS spectrum of Cr^{3+} in water using a different computer simulation of the system but reached similar conclusions.

In this work, we aim at establishing quantitative relationships of more general validity by studying the Rh^{3+} hydration to enable its application to a series of di- and trivalent hexahydrated aquaions. Differences between chromium and rhodium EXAFS data are analyzed. They supply a general manner to assign structural and spectroscopic effects. Calculated XANES spectra are compared with experimental ones. Information about the second hydration shell in the spectrum is analyzed from different points of view. The benefits of combining the spectroscopic information contained in the XAS spectra and the microscopic details supplied by MD simulations is explored. The aim was to get insight into the possibilities of simultaneously providing an average structure in aqueous solution and determining how large the fluctuations around this structure are as a consequence of the molecular motion in solution.

Methods

MD Simulations. K-edge XAS spectra of Cr^{3+} and Rh^{3+} cations in water were calculated from snapshots of MD simulations. The interaction potentials employed for the simulation were based on a flexible hydrated ion model. Two types of water molecules are considered. First-shell water molecules, $(H_2O)_I$, are the highly perturbed water molecules in the closest environment of the trivalent cation. Thus, $Cr^{3+}-(H_2O)_I$ interactions were described by an effective ion−water first-shell potential (IW1).[23] A second type of water molecules are those forming the bulk, $(H_2O)_{bulk}$, that interact with the hydrated ion by means of the hydrated ion water (HIW) potential. Thus, $[Cr(H_2O)_6]^{3+}-(H_2O)_{bulk}$ interactions were described by the HIW potential.[24,25] Bulk water−water interactions were described by the TIP4P potential.[26] The Rh^{3+} potentials were built using a method previously suggested by our group that assumes transferability of some contributions from a thoroughly studied cation.[25] This procedure was applied successfully to Al^{3+}, Mg^{2+}, and Be^{2+}.[27] Details about the potential are given as Supporting Information. The elementary simulation cell contained 1 M^{3+} + 6 $(H_2O)_I$ + 512 $(H_2O)_{bulk}$. Long-range interactions were incorporated by means of the Ewald summation. A specific term accounting for the charged system is incorporated in the treatment. The correctness of this procedure has been reported by several authors,[28,29] and its particularly good behavior in the cases studied has also been shown elsewhere.[21−23,27] One nanosecond of simulation at 298 K was performed in the microcanonical ensemble.

EXAFS Spectrum Computations. Simulation provided snapshots evenly spaced in time for the analysis of the EXAFS part. When summing over MD structures, eq 1 is in fact slightly modified, because the disorder arises from summing over a number of MD structural arrangements:

$$\chi(k) = \frac{1}{N_s}\sum_{l}^{N_s}\sum_{j'}^{\text{paths}} \frac{N_{j'} S_0^2}{kR_{lj'}^2} |f^{\text{eff}}(k,R)| \times \sin(2kR_{lj'} + \varphi_{j'}(k))\, e^{-2R_{lj'}/\lambda} \quad (2)$$

where N_s is the number of structures considered (unless stated otherwise, 500 structures were used), l goes over the structures obtained from the statistical sampling, and j' goes over the paths.

For each structure, a cutoff centered around the metal atom was applied to include water molecules whose oxygen atoms lie at distances up to 7.0 Å. That way, more than two hydration shells were included. At these distances, the radial distribution functions (RDFs) are close to 1. Paths with a length of up to 7.0 Å were included. XAS calculations

(10) Jalilehvand, F.; Spångberg, D.; Lindqvist-Reis, P.; Hermansson, K.; Persson, I.; Sandström, M. *J. Am. Chem. Soc.* **2001**, *123*, 431.
(11) Campbell, L.; Rehr, J. J.; Schenter, G. K.; McCarthy, M. I.; Dixon, D. *J. Synchrotron Radiat.* **1999**, *6*, 310.
(12) D'Angelo, P.; Barone, V.; Chillemi, G.; Sanna, N.; Meyer-Klauche, W.; Pavel, N. V. *J. Am. Chem. Soc.* **2002**, *124*, 1958 and references therein.
(13) Westre, T. E.; Kennepohl, P.; DeWitt, J. G.; Hedman, B.; Hodgson, K. O.; Solomon, E. I. *J. Am. Chem. Soc.* **1997**, *119*, 6297.
(14) Natoli, C. R.; Benfatto, M.; Brouder, C.; Ruiz López, M. F.; Foulis, D. L. *Phys. Rev. B* **1990**, *42*, 1944.
(15) Ohtaki, H.; Radnai, T. *Chem. Rev.* **1993**, *93*, 1157.
(16) Helm, L.; Merbach, A. E. *Coord. Chem. Rev.* **1999**, *187*, 151.
(17) Muñoz-Páez, A.; Pappalardo, R. R.; Sánchez Marcos, E. *J. Am. Chem. Soc.* **1995**, *117*, 11710.
(18) Muñoz-Páez, A.; Sánchez Marcos, E. *J. Am. Chem. Soc.* **1992**, *114*, 6931.
(19) Hasnain, S. S.; Murphy, L. M.; Strange, R. W.; Grossmann, J. G.; Clarke, A. R.; Jackson, G. S.; Collinge, J. *J. Mol. Biol.* **2001**, *311*, 467.
(20) Sakane, H.; Muñoz-Páez, A.; Díaz-Moreno, S.; Martínez, J. M.; Pappalardo, R. R.; Sánchez Marcos, E. *J. Am. Chem. Soc.* **1998**, *120*, 10397.
(21) Merkling, P. J.; Muñoz-Páez, A.; Martínez, J. M.; Pappalardo, R. R.; Sánchez Marcos, E. *Phys. Rev. B* **2001**, *64*, 012201.
(22) Merkling, P. J.; Muñoz-Páez, A.; Pappalardo, R. R.; Sánchez Marcos, E. *Phys. Rev. B* **2001**, *64*, 092201.
(23) Martínez, J. M.; Pappalardo, R. R.; Sánchez Marcos, E. *J. Chem. Phys.* **1998**, *109*, 1445.
(24) Pappalardo, R. R.; Sánchez Marcos, E. *J. Phys. Chem.* **1993**, *97*, 4500.
(25) Martínez, J. M.; Pappalardo, R. R.; Sánchez Marcos, E.; Refson, K.; Díaz-Moreno, S.; Muñoz-Páez, A. *J. Phys. Chem. B* **1998**, *102*, 3272.
(26) Jorgensen, W. L.; Impey, R. W.; Chandrasekhar, J.; Madura, J. D.; Klein, M. L. *J. Chem. Phys.* **1983**, *79*, 926.
(27) Martínez, J. M.; Pappalardo, R. R.; Sánchez Marcos, E. *J. Am. Chem. Soc.* **1999**, *121*, 3175.
(28) Leslie, M.; Gillan, M. I. *J. Phys.: Condens. Matter* **1985**, *18*, 973.
(29) Hummer, G.; Pratt, L. R.; Garcia, A. E. *J. Phys. Chem. A* **1998**, *102*, 7885.

were performed with the FEFF program (version 8.10).[30] A path decomposition was performed, and very low intensity paths were filtered out. The subsequent application of FEFFIT[31] (version 2.54) yielded the spectra in k and r spaces.

The contribution of hydrogen atoms to the computation of the EXAFS signal can be separated into two components: first, the role played when the potentials of the oxygen atoms are computed, and second, their own contribution to the scattering phenomena. Whereas the first component is well accepted, the second one is usually neglected, based on the low scattering factor of hydrogen atoms. Thus, Benfatto et al.[32] find that hydrogen contribution is not significant in the case of EXAFS. Likewise, Palmer et al.,[6] Rehr and colleagues,[11] Sandström and colleagues,[9,10] and our group[21,22] have been reluctant to include hydrogen contribution, as far as it seems to be generally overestimated by the current models. On the other hand, D'Angelo et al.[12] have proposed that the inclusion of hydrogen scattering phenomena is essential to perform a quantitative EXAFS analysis of ionic aqueous solutions. A structural analysis where the number of parameters is increased and their associated contributions are overestimated, as could be the case derived from hydrogen inclusion, might affect the results due to the non-well-balanced contributions to the XAS spectra. In this work, we have revisited this point by generating an EXAFS signal from the MD structures including and excluding the scattering contributions of hydrogen atoms. In this way, we attempt to settle the boundaries of this controversial point within the methodology here employed. A comparison among the phase-shift-corrected FT of the EXAFS function corresponding to the Cr^{3+} hydration case has been made when hydrogen atoms have been (a) considered in the computation of the potential of the oxygen atoms or (b) considered in the whole computation. The results have been summarized in Figure S1, included as Supporting Information. It is shown that the scattering contribution from hydrogen atoms is small enough to justify the use of the intermediate approach, that is, considering the hydrogen atoms to compute the different potentials but excluding scattering paths which include hydrogen atoms.

Considering core hole lifetimes for both cations[33] and monochromator resolutions, the broadenings were set to 0.4 eV for Cr and 0.6 eV for Rh. The free parameters of the fit were the distances (R_I and R_{II}) and DW factors (σ_I^2 and σ_{II}^2), as well as the inner potential correction ΔE_0 used to obtain k. All paths from Figure 1, as well as three four-legged triangular paths (see Figure 3 in ref 20), were considered. Model calculations using a geometry close to the fitted geometry enabled extending the k range to low values ($k \leq 3$ Å^{-1}), which is especially important if high-frequency contributions are examined. The ranges employed were therefore $\Delta k = 2.4-13.7$ Å^{-1} for Cr and 2.5−12.7 Å^{-1} for Rh.

A practical question when dealing with the computation of spectra from MD simulations is the determination of the sampling interval and total sampling length. Therefore, we determined EXAFS averages over restricted regions of the phase space. Four separate spectra were calculated from four independent series of 500 configurations taken over a total simulation range of 5 ps. At the other extreme, to check that the choice of 500 configurations used in all our calculations provides a correct sampling, another calculation was performed over the whole simulation range of 1 ns using 25 000 configurations. The Supporting Information includes Figure S2 that shows the FT of the computed Rh EXAFS spectrum for different samplings. Results show that too short simulation times may lead to systematic errors in the EXAFS signal due to insufficient sampling. On the contrary, the choice of 500 configurations distributed equally over 1 ns to build an average spectrum is in fair agreement with the spectrum averaged over 25 000 configurations. Thus, 500 configurations is the lower limit if determination of structural parameters of the second shell is the aim. Tentatively, structural parameters were extracted from the averages over the restricted time regions (500 configurations over 5 ps). They all led to essentially equivalent parameters, although the uncertainties found were larger (for instance, under less optimized fitting conditions, second-shell parameters of $R_{ss2} \approx 4.5$, $\sigma_{ss2} \approx 0.019$ were obtained for some of the series; these values are very different from the real simulation values in Table 1), reflecting the sensitivity of the determination of structural parameters to fluctuations in the EXAFS signal. It is worth emphasizing that in this model, reducing the quality of the statistical sampling leads ultimately to nonphysical data because the fitting process becomes unstable. This might be compared to the problems that occur when poor-quality experimental data are used.

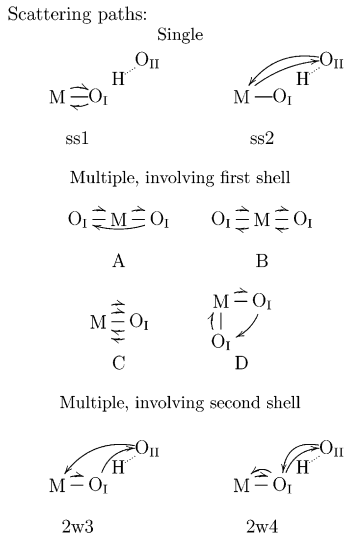

Figure 1. Main scattering paths contributing to the EXAFS spectrum: first and second hydration shell single scattering and first-shell multiple scattering (MS) at the oxygen sites.

XANES Spectrum Computations. One hundred snapshots evenly spaced in time for the computation of the XANES spectrum were used. The cutoff radius to define the cluster size was chosen to be 7.0 Å, as in EXAFS calculations. XANES calculations used the Hedin−Lundqvist potential applied to muffin-tin potentials. The electron density distribution was obtained self-consistently. The maximum angular momentum l needed was found to be at least 3 on chromium and 4 on rhodium, and an SCF radius centered on each type of atom was set to 4.5 Å. Atoms at distances >4.5 Å from the absorber atom modify the potential experienced by first- and second-shell oxygen atoms. Two types of oxygen atoms were considered in the calculations, first-shell and "other" oxygen atoms. Because of the region sampled by the photoelectron in XANES, i.e., its mean free path is larger than in EXAFS, full multiple scattering calculations (FMS) were performed within a sphere of 4.5 Å around the cation. More details may be found in ref 22. As in the case of EXAFS, hydrogen atoms were employed only to obtain the oxygen potentials.

Experimental Spectra. The experimental EXAFS and XANES spectra used in this work for 0.1 M aqueous solutions of chromium and rhodium nitrate were measured at wiggler beam-line 9.2 of the SRS in Daresbury, U.K. (Rh K-edge, 23 220 eV) and at beam-line BL-12C of Photon Factory in Tsukuba, Japan (Cr K-edge, 5989 eV). Further details may be found in ref 20. The additional Rh K-edge XANES spectrum with increased energy resolution was recorded at the ESRF (Grenoble, France), beam-line BM29, with ring energy 6 GeV, ring current 175 mA, and using a Si(311) double-crystal monochromator, detuned 50% to reject higher harmonics. Energy calibration was done with a Rh foil. Energy resolution is estimated to be about 1.2 eV. Measurements were carried out in transmission mode using optimized

(30) Ankudinov, A.; Ravel, B.; Rehr, J. J.; Conradson, S. D. *Phys. Rev. B* **1998**, *58*, 7565.
(31) Stern, E. A.; Newville, M.; Ravel, B.; Yacoby, Y.; Haskel, D. *Physica B* **1995**, *208−209*, 117.
(32) Benfatto, M.; Solera, J. A.; Chaboy, J.; Proietti, M. G.; García, J. *Phys. Rev. B* **1997**, *56*, 2447.
(33) Krause, M. O.; Oliver, J. H. *J. Phys. Chem. Ref. Data* **1979**, *8*, 329.

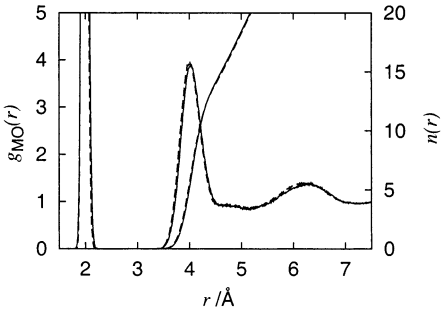

Figure 2. Metal−oxygen radial distribution functions and running coordination numbers extracted from MD simulation: Rh^{3+} (dashed line) and Cr^{3+} (solid line).

ion chambers filled with He/Ar for I_0 and He/Kr for I_1 detection. Data points were collected for 1 s each, and, to improve the signal-to-noise ratio, several scans were recorded and averaged. The Ni K-edge (8333 eV) of a 0.1 M nickel nitrate aqueous solution was measured at beamline 8.1 of the SRS in Daresbury, UK.[34]

Results

MD Analysis. The direct information employed to compute the XAS spectra was that obtained from MD simulations via a large number of evenly spaced snapshots. The metal−oxygen (M−O) radial distribution functions (RDFs), where M = {Cr, Rh}, is represented in Figure 2. The chromium and rhodium hydration structures obtained from the simulation are similar. The maxima of the first peak corresponding to the M−O RDFs are 2.00 ± 0.01 (Cr) and 1.99 ± 0.01 Å (Rh). The maxima of the second peak appear at 4.02 ± 0.05 (Cr) and 4.00 ± 0.05 Å (Rh), and the integration numbers for these peaks are 14 ± 0.5 water molecules. To define the second hydration shell, we adopted the following criterion: a water molecule belongs to this shell when its oxygen atom is separated from the metal cation by a distance between 3.0 and 4.5 Å (the values of the minima delimiting the second peak of the M−O RDFs). The MD results agree well with experimental information available in the literature.[15,35] Apart from the structural information, the Cr^{3+}−water interaction potentials have been satisfactorily tested in previous works, where dynamics, energetic, and spectroscopic results were thoroughly examined.[23,25,36,37] A detailed analysis of different properties of the simulated Rh^{3+} aqueous solution supports the new Rh^{3+}−water interaction potentials.[38]

EXAFS Spectrum. Figure 3 shows a comparison of experimental and calculated EXAFS functions. [For the purpose of the representation in *k*-space, an inner potential correction of −6 eV was applied to the chromium spectrum and −3 eV for the rhodium.] Amplitude reduction factors S_0^2 were 0.81 and 0.80 for chromium and rhodium, respectively. These factors were obtained empirically to match the first peak height in the FT but constitute per se a useful piece of information. The agreement of the spectra is satisfactory. We note, however, that the position of the main peak in the FT is slightly shifted for the rhodium spectrum. This can be due to a mismatch in $M-O_I$ distance.

Quantitative structural information is contained in the EXAFS part of the spectrum, as expressed by eq 1. To analyze the relative importance of scattering paths, their contributions to the EXAFS function were considered separately. The most relevant scattering paths are shown in Figure 1. During the fitting of an experimental spectrum, an average model structure, such as that shown in Figure 4, is usually considered. In this case, the relevant scattering paths are highly degenerate. When the spectrum is computed from MD simulations, fluctuations in atomic positions along the selected snapshots result in nonsymmetric arrangements, most degeneracies of the paths are removed, and the number of different paths increases drastically. Nevertheless, even in this case, it is useful to group the paths according to Figure 1 to rationalize the results. Structural parameters of the most important paths derived from the MD simulation, grouped as in Figure 1, are given in Table 1. It must be pointed out that the *R* data for the different paths were obtained as an averaged value from snapshots of the MD simulations, $\bar{R}$. The ss2 values, which correspond to the second hydration shells, are larger than those corresponding to the maximum of the second shell in the M−O RDFs due to the asymmetry of these peaks. For the sharp and symmetric first peaks, the values for $\bar{R}$ and the maximum of the RDFs match.

The main contribution to the spectra in Figure 3a.2 and 3b.2 is due to the first-shell single scattering path (ss1). Paths A, B, C, and ss2, with very similar path lengths (see *R* values in Table 1), roughly twice the MO_I distance, interact either constructively or destructively. Their sum yields the peak at around 4 Å in the FT spectrum.[11] Other paths, which represent minor contributions but might affect the phase of the signal, are indicated as well. Two of these, 2w3 and 2w4, are multiple scattering paths involving oxygen atoms of the first- and second-shell water molecules connected by hydrogen bonds.

For the total signal of FTs shown in Figure 3, the ratio $I(r = 2^{nd}\ max)/I(r = 1^{st}\ max)$ is lower in rhodium than in chromium (by ∼20%). However, in both rhodium and chromium, the contributions involving the second shell are of similar importance relative to the total amplitude of the second peak. This can be seen in Figure 5, where the amplitudes for first-shell multiple scattering and the ones for the second shell are separated. Likewise, in *r*-space the second-shell contribution represents roughly 35% of the total amplitude for both cations. Consequently, a similar reliability or accuracy in the determination of structural parameters for rhodium and for chromium is expected.

Computer simulations provide us with detailed microscopic information that can otherwise be hard to estimate. In particular, the calculation of EXAFS spectra from an idealized model structure (Figure 4) should include parameters that account for the static and dynamic disorder. For any given type of path, this may be expressed by the *l*th-order cumulants of the distribution of (disordered) structures:

$$\sigma_j^{(l)} = \frac{1}{n_j}\sum_{i=1}^{n_j}(R_{i,j} - \bar{R}_j)^l$$

These have been calculated from the simulation, and their

(34) Díaz-Moreno, S.; Muñoz-Páez, A.; Sánchez Marcos, E. *J. Phys. Chem. B* **2000**, *104*, 11794.
(35) Magini, M.; Licheri, G.; Paschina, G.; Piccaluga, G.; Pinna, G. *X-ray Diffraction of Ions in Aqueous Solutions: Hydration and Complex Formation;* CRC Press: Boca Raton, FL, 1988.
(36) Pappalardo, R. R.; Martínez, J. M.; Sánchez Marcos, E. *J. Phys. Chem.* **1996**, *100*, 11748.
(37) Martínez, J. M.; Hernández-Cobos, J.; Saint-Martin, H.; Pappalardo, R. R.; Ortega-Blake, I.; Sánchez Marcos, E. *J. Chem. Phys.* **2000**, *112*, 2339.
(38) Martínez, J. M.; Pappalardo, R. R.; Refson, K.; Sánchez Marcos, E. To be published.

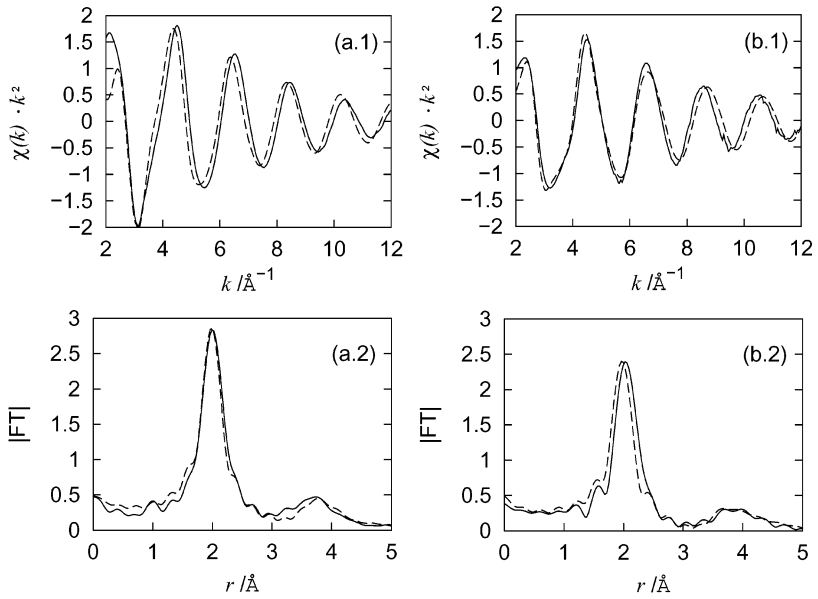

Figure 3. Cr (a.1) and Rh (b.1) K-edge EXAFS spectra and the amplitudes of their phase-corrected FT (a.2 and b.2, respectively). Experimental spectra are shown in solid lines, calculated ones in dashed lines.

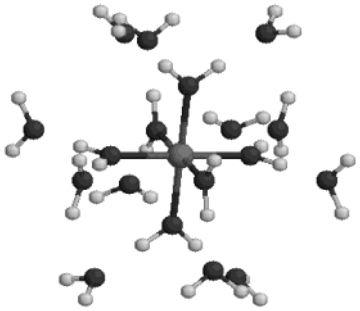

Figure 4. Model structure used for the purpose of adjusting structural parameters.

Table 1. Distances, Second-Order Cumulants, and Amplitude Reduction Factor Obtained from MD Simulation

	Cr ($S_0^2 = 0.81$)			Rh ($S_0^2 = 0.80$)		
path	*N*	*R*/Å	σ^2/Å^2	*N*	*R*/Å	σ^2/Å^2
ss1	6.00	2.000	0.0024	6.00	1.989	0.0018
ss2	14.0	4.080	0.0394	13.88	4.062	0.0411
A	5.96	3.996	0.0044	5.97	3.975	0.0033
B	5.96	3.999	0.0044	5.97	3.978	0.0033
C	6.00	3.999	0.0097	6.00	3.978	0.0072
D	23.99	3.412	0.0045	23.98	3.395	0.0039
2w3	23.53	4.318	0.0168	23.51	4.309	0.0168
2w4	11.77	4.581	0.0142	11.76	4.583	0.0139
O_IO_{II}	11.82	2.585	0.0134	11.80	2.598	0.0138

averages are presented in Table 1. In this formula, n_j represents the number of *j*-type paths found along the selected snapshots and $\overline{R_j}$ is the length of path *j* averaged over the whole simulation. For both rhodium and chromium, there are 6 molecules in the first coordination shell of the metal cation and roughly 14 in the second. Approximately 12 of the latter are hydrogen-bonded to first-shell water molecules, as seen from the *N* values corresponding to 2w4 and O_IO_{II}. The second-order cumulant, which is identical to the DW factor from EXAFS theory (see eq 1), is indicative of the symmetrical disorder around the average value. The DW factor of the ss1 path is smaller by 25% in rhodium than in chromium. Approximately the same relation holds for paths A−D. The idea that Debye−

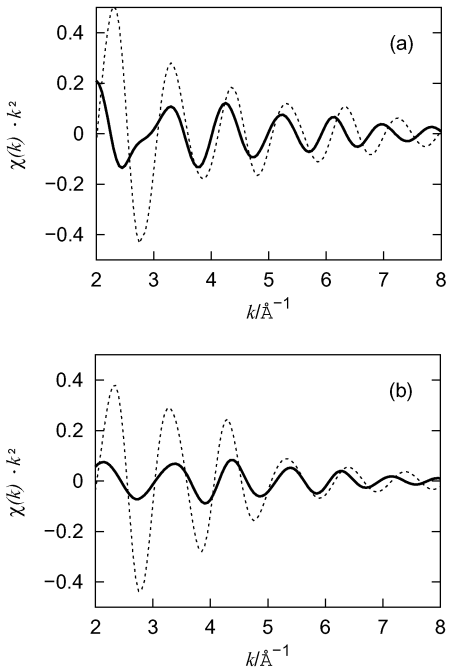

Figure 5. Contributions to the *k*-space EXAFS spectrum for Cr and Rh: second-shell scattering (solid lines) and first-shell multiple scattering (dotted lines).

Waller factors of multiple scattering paths depend in a simple multiplicative way on those of single scattering paths is elegantly developed by Yokoyama et al. in their model of independent vibrations,[39] and its implementation for the case of a hydrated ion in solution has been fruitful.[21,20] An examination of the σ^2 values of Table 1 corroborates these rules. Paths involving the second shell are very similar in chromium and rhodium. Third-order cumulants are all found to be small, especially for first-shell paths, indicating that the distribution in the simulation is symmetrical around its maximum. Fourth-order cumulants are

(39) Yokoyama, T.; Kobayashi, K.; Ohta, T.; Ugawa, A. *Phys. Rev. B* **1996**, *53*, 6111.

Table 2. Distances and Debye−Waller Factors around Metal Cation Obtained by Fitting a Spectrum of a Model Structure Either to the EXAFS Spectrum Computed from MD Structures (A) or to the Experimental One (B)

	A		B[a]	
path	*R*/Å	σ^2/Å^2	*R*/Å	σ^2/Å^2
		Cr		
R-factor	0.0003		0.022	
ss1	1.999	0.0023	1.967	0.0027
	±0.001	±0.0001	±0.004	±0.0003
ss2	4.01	0.030	4.02	0.028
	±0.01	±0.001	±0.04	±0.009
		Rh		
R-factor	0.0018		0.025	
ss1	1.987	0.0019	2.016	0.0012
	±0.001	±0.0001	±0.004	±0.0003
ss2	4.00	0.032	3.99	0.024
	±0.02	±0.004	±0.06	±0.011

[a] EXAFS data from ref 20.

also small. Third- and fourth-order cumulants are given as Supporting Information.

A striking fact in this table is that the DW factors of paths 2w3 and 2w4 are smaller than that of path ss2. Similar behavior has already been observed by Campbell and Rehr[40] in their Cr^{3+} in water study. The origin of the behavior of DW factors of the second shell is analyzed in more detail in the Discussion section.

The structural data given in Table 1 are obtained directly from atomic positions of the MD simulation. Another way of obtaining these geometrical parameters is by performing data analysis of an EXAFS spectrum. The standard method is to carry out a fit to eq 1 of an EXAFS spectrum. Method A in Table 2 is a fit to eq 1 of the computed EXAFS spectrum shown in Figure 3, which was calculated through eq 2 based on MD simulation data. This procedure is a direct test of the reliability of the information retrieved from an EXAFS spectrum. It is of interest to check how close these values are from those collected in Table 1, which are in fact the "exact values". The indetermination given in Table 2 is that derived from the fitting procedure. Method B uses an experimental EXAFS spectrum to obtain structural data. For both methods, DW factors of multiple scattering paths of the first shell were assumed to be proportional to path ss1, and those of the second shell proportional to path ss2. The proportionality factors were extracted from the simulation values in Table 1. The extraction of structural data from the spectrum (method A in Table 2) reveals that the first-shell parameters are obtained accurately: distances within 0.001 (Cr) or 0.002 (Rh) Å and σ^2 within 0.0001 Å^2. In the case of the second shell, the distance is found to be 0.07 (Cr) or 0.06 (Rh) Å shorter. DW factors are underestimated by 25%. These differences can be considered as methodological errors associated with the fitting procedure itself.

The fit of the experimental spectra yields $M-O_I$ distances of 1.97 Å for Cr and 2.02 for Rh, that is, 0.03 Å shorter and 0.03 Å larger than the simulation values for Cr and Rh, respectively. This is probably attributable to the intermolecular potentials used in the simulation. DW factors are in better agreement in the case of chromium than in the case of rhodium. This difference might be also related to the intermolecular potential. It might be due as well to a bad estimate of the

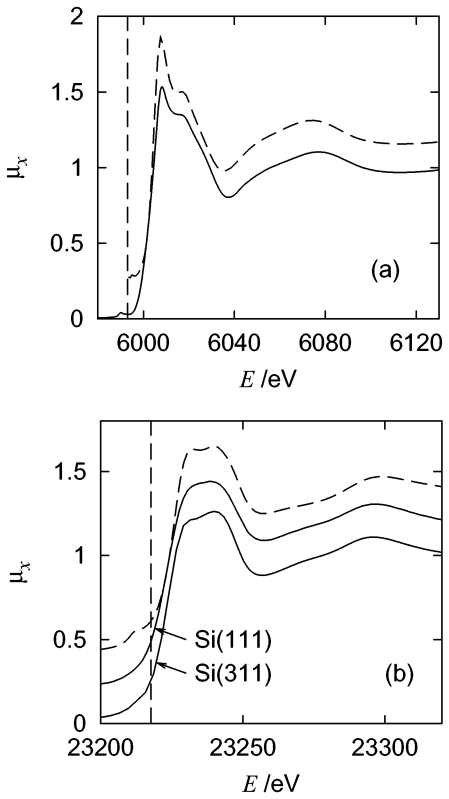

Figure 6. Cr (a) and Rh (b) K-edge XANES experimental (solid line) and calculated (long-dashed) spectra (for computational details, see text). The dashed vertical line indicates the Fermi level of the calculated spectrum.

experimental energy broadening, which is set to zero in method A but has to be estimated in method B (see Methods section). Second-shell distances and DW factors agree with those determined by the EXAFS spectra computed from MD. Cr and Rh second shells are found to have similar parameters. The slightly larger indetermination in the parameters of the Rh structure is not significant. The fitting parameters agree reasonably well with those of ref 20. The inclusion of σ^3 values from the simulation did not affect the results for both ions and types of spectra.

XANES Spectra. The calculated chromium and rhodium spectra are compared with their experimental counterparts in Figure 6. The agreement with the experimental spectra is fairly good for both cations. As predicted by computations, the experimental rhodium spectrum exhibits a slight splitting of the main edge resonance. [The experimental Rh K-edge spectrum obtained using a Si(111) monochromator was measured by our group in 1993. The calculated absorption spectrum was generated in Spring 2001. It exhibited a splitting of the main edge resonance not present in the first experimental spectrum. We wondered whether this discrepancy could be due to a low-energy resolution of the monochromator, because the maxima of the peaks were separated by 8−9 eV and the natural width is around 6 eV.[33] To confirm this, an experimental spectrum with higher resolution (using a Si(311) monochromator) was recorded in September 2001 at the ESRF, Grenoble.] The relative position of the peaks and the shape of the curve at energies above 23 250 eV agree with the theoretical calculation. Although in chromium the calculated edge energy agrees well with the experimental one (±1), the absolute position of the rhodium spectrum is 27 eV off from the experimental one, which represents a relative

(40) Campbell, L.; Rehr, J. "Cr hydrates", 1998 draft report, unpublished.

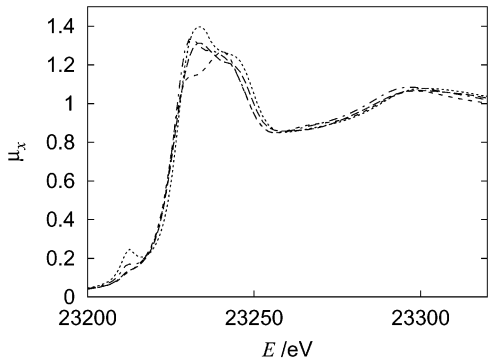

Figure 7. Individual Rh-K-edge XANES spectra computed for different snapshots.

shift of 0.1%. This reflects the difficulty in estimating accurately the absolute energy of the Fermi level by quantum mechanics, when heavier atoms and inner electrons are involved in the ionization processes.[30] Given these difficulties, some computer codes work with relative values.[41−45]

On average, first-shell oxygen atoms adopt an octahedral symmetry around the absorber atom (Cr and Rh); therefore, experimental spectra have low-intensity pre-edge features. In Cr it is a small peak, and in Rh it is simply a "bump" at the base of the rising edge. As previously reported, the position of the pre-edge and of the Fermi level in the calculation is found closer to the edge than in the experiment.[46]

Significant differences appear in the shape of the spectrum before the rising edge among the individual XANES spectra of rhodium corresponding to selected snapshots (see Figure 7). Note that, in the region of the "bump" of the averaged spectrum (Figure 6b), some of the individual spectra exhibit almost no pre-edge feature, while others show a well-defined one. As expected, the geometry of the first hydration shell corresponding to these structures is a distorted octahedron.

Discussion

Second Hydration Shell and Spectroscopic Atomic Effects. The good reproduction of EXAFS spectra obtained for the cations Cr^{3+} and Rh^{3+} in water on the basis of MD simulations proves that the proposed methodology employs an accurate enough model of the statistics of the solution and of its spectroscopic properties. Taking advantage of these results, it is worth undertaking a detailed analysis of the capability of determining the second hydration shell as a function of the atomic number. Al, Cr, Fe, Ni, Rh, and Ir were taken as absorber atoms. One way of checking this effect is to carry out the computation of EXAFS spectra from the MD simulation snapshots of the Cr^{3+} aqueous solution, but replacing this cation by other metal cations in the spectroscopic calculations. The EXAFS functions obtained corresponding to the K- or L_3-edges are then fitted to a model structure as in method A from Table 2. For each cation considered, the fit results have to be compared with those of the Cr^{3+} MD simulation indicated in Table 1. This strategy allows the clear separation of the structural contributions from the spectroscopic ones, as well as an estimation of the reliability of the determination of second-shell parameters. The calculated EXAFS functions are strongly dependent on the absorber atom because the relative amplitudes of the paths vary. For instance, for Cr^{3+} and Rh^{3+}, the amplitude of path B is higher than that of path A, whereas for the case of Ni^{2+}, whose spectrum is presented later, the situation is reversed.

Table 3. Distances and Debye−Waller Factors around Metal Cation Obtained from Fitting to Computed EXAFS Spectra Based on the Same Set of Geometries Taken from the MD Simulation of Chromium: $\overline{R_{ss1}} = 2.000$ Å, $\overline{\sigma_{ss1}{}^2} = 0.0024$ Å^2, $\overline{R_{ss2}} = 4.078$ Å, and $\overline{\sigma_{Ss2}{}^2} = 0.00388$ Å^2 [a]

atom	E/eV	R_{ss1}/Å	$\sigma_{ss1}{}^2$/Å^2	R_{ss2}/Å	$\sigma_{ss2}{}^2$/Å^2
Al	1559	2.001	0.00234	4.022	0.0313
		±0.0009	±0.00007	±0.01	±0.0025
Cr	5989	1.999	0.00232	4.012	0.0301
		±0.0005	±0.00004	±0.005	±0.0011
Fe	7112	2.000	0.00234	4.021	0.0324
		±0.001	±0.00008	±0.011	±0.0026
Ni	8333	2.000	0.00234	4.022	0.0327
		±0.0011	±0.00009	±0.012	±0.0030
Ir-L3	11215	2.000	0.00232	4.020	0.0317
		±0.0012	±0.00009	±0.018	±0.0040
Rh	23220	1.999	0.00232	4.010	0.0321
		±0.0004	±0.00003	±0.008	±0.0014
Ir	76111	1.998	0.00233	4.027	0.0294
		±0.0002	±0.00001	±0.038	±0.0062

[a] These values differ slightly from those in Table 1 due to averaging over a smaller number of structures (500).

Table 4. Recommended Ratios of DW Factors between Paths To Be Applied for the Fitting of a Spectrum of a Species with Octahedral Coordination in Aqueous Solution

	A	B	C	D	2w3
$\sigma_i{}^2/\sigma_{ss1}{}^2$	2.0	2.0	4.0	2.0	
$\sigma_i{}^2/\sigma_{ss2}{}^2$					0.45

The results of the subsequent EXAFS signal fitting are summarized in Table 3. Similar structural parameters were obtained for all central atoms probed, and even the uncertainties on the determination are comparable. Although the contribution to the EXAFS function due to the second hydration shell is small, it is coherent enough to be analyzed reliably. Consequently, the conclusion derived from this analysis is that the possibility of determining the second shell does not depend primarily on the spectroscopic properties of the absorber atom. In any case, it must be recalled that the highly structured system chosen for this analysis favors the determination of the second hydration shell.

An important advantage of dealing with a microscopic description of the solution is the information derivable from fluctuations around the absorber atom. This enables a priori estimation of DW factors for the paths, thus simplifying the fitting procedure by eliminating highly correlated fit parameters. Following the idea of Yokoyama et al.,[39] we have quantified the ratio of DW factors of multiple scattering paths over those of the simple scattering paths for octahedrally coordinated metal cations. Table 4 sums up the most relevant constraints that correspond to relationships valid in the case of chromium and found to be virtually unchanged in the case of rhodium. Although further trials are necessary, we expect these results

(41) Natoli, C. R.; Benfatto, M. Unpublished data.
(42) Tyson, T. A.; Hodgson, K. O.; Natoli, C. R.; Benfatto, M. *Phys. Rev. B* **1992**, *46*, 5997.
(43) Della Longa, S.; Soldatov, A.; Pompa, M.; Bianconi, A. *Comput. Mater. Sci.* **1995**, *4*, 199.
(44) Bugaev, L. A.; Ildefonse, P.; Flank, A.-M.; Sokolenko, A. P.; Dmitrienko, H. V. *J. Phys.: Condens. Matter* **1998**, *10*, 5463.
(45) Durham, P. J.; Pendry, J. B. *Comput. Phys. Commun.* **1982**, *25*, 193.
(46) Farges, F.; Brown, G. E., Jr.; Rehr, J. J.; Conradson, S. D. *Phys. Rev. B* **1997**, *56*, 1809.

Table 5. Distances and Debye−Waller Factors around Ni^{2+} in Water Obtained from Fitting an Experimental EXAFS Spectrum Using the Coefficients of Table 4[a]

	this fit		other EXAFS	
path	*R*/Å	σ^2/Å^2	*R*/Å	σ^2/Å^2
R-factor	0.021			
ss1	2.051 ±0.006	0.0061 ±0.0004	2.05−2.07	0.0016−0.0055
ss2	3.99 ±0.05	0.042 ±0.012		

	XRD		neutron diffraction	
path	*R*/Å	σ^2/Å^2	*R*/Å	σ^2/Å^2
ss1	2.04−2.15	0.008−0.020	2.05−2.10	0.017
ss2	3.99−4.33	0.044−0.31		

[a] Conditions were $\Delta k = 2.8-12.7$ Å^{-1}. They are compared to determinations from different techniques found in ref 15.

to be of general validity for cations in octahedral environment in solution. Due to the intrinsic correlation of DW factors and S_0^2, the determination of DW factors from a source other than XAS reduces the number of strongly coupled parameters in the fitting procedure. In addition to these recommended ratios between DW factors, a value of S_0^2 is proposed for these hexahydrated metal cations.

Experimental Fitting of an EXAFS Spectrum of a Ni^{2+} Aqueous Solution. The relationships in Table 4 were applied to an experimental spectrum of an aqueous Ni^{2+} solution. The fit parameters obtained, shown in Table 5, are within the broad range given by other experimental EXAFS, X-ray diffraction (XRD), and neutron diffraction studies.[15] Until now, XRD has been the principal source of structural information about the second shell, although the wide range of values published indicates that it is not exempt from arbitrariness. In fact, the second shell represents a minor contribution which usually is overlapped by others. As a consequence, its associated parameters are obtained by applying techniques such as the isomorphous substitution method: to isolate partial distribution functions, the central ion studied is replaced by another ion assumed to be structurally equivalent.[35,47] Although EXAFS amplitude decays more rapidly with distance, the number of independent pair contributions is also highly reduced with respect to diffraction techniques. This draws a scenario in EXAFS analysis where the second hydration shell contribution is relatively important within minor contributions, whereas in the scattering analysis this second hydration shell contribution, though more intense, is smeared out by many other contributions at these distances from the central cation. Paradoxically, the high accuracy of EXAFS in the structural determination of the first shell might have contributed to the judgement that EXAFS is inappropriate for second-shell determination in water.[48,35] However, first- and second-shell distances in this determination and most other ones agree.[15] When compared with data obtained in the fit of chromium or rhodium (Table 1), this fitting gives a realistic value. DW factors obtained by us are consistent with values obtained from XRD for the related parameter, mean square deviation.[15,35]

Relationships among Fluctuations of Geometrical Parameters and DW Factors of Selected Paths. Simulation results

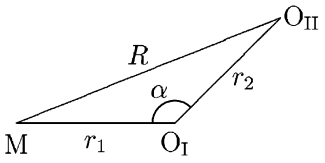

Figure 8.

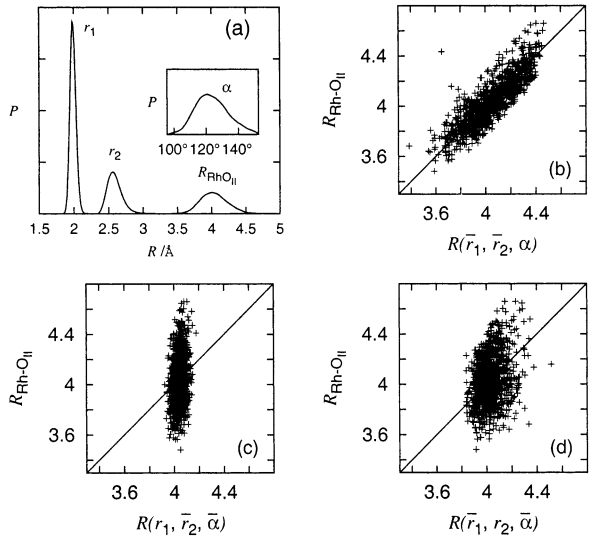

Figure 9. Probability distributions of the $R_{Rh-O_{II}}$, $\alpha = \angle RhO_IO_{II}$, $r_1 = Rh-O_I$, and $r_2 = O_I-O_{II}$ values in simulation snapshots (a). Correlations between the $Rh-O_{II}$ distance and its angle $\alpha = \angle RhO_IO_{II}$ (b), $r_1 = Rh-O_I$ (c), or $r_2 = O_I-O_{II}$ (d) that is converted to an $Rh-O_{II}$ distance using eq 3 and averaged values $\bar{r}_1$, $\bar{r}_2$ (b), $\bar{r}_2$, $\bar{\alpha}$ (c), or $\bar{r}_1$, $\bar{\alpha}$ (d).

presented in Table 1 had revealed that surprisingly low DW factors were obtained for paths 2w3 and 2w4 (Figure 1); thus, the contribution of path 2w3 has to be taken into account in the calculation of the EXAFS signal. As expected for the strong interaction between a trivalent cation and a water molecule in its first hydration shell, the DW factor of the MO_I distance (path ss1) is small. The DW factor of the O_IO_{II} distance was also found to be relatively small, indicating a strong binding due to the hydrogen bond. Since the fluctuations of both distances are small but the DW factor of path ss2 is rather large, the angle between the vectors must be fluctuating greatly. This conclusion can be validated if one considers the triangle MO_IO_{II} (Figure 8) and computes the probability functions as well as the average values for $r_1 = R_{MO_I}$ and $r_2 = R_{O_IO_{II}}$ and $\alpha = \angle MO_IO_{II}$. Figure 9a plots the probability functions for the three distances r_1, r_2 and $R_{MO_{II}}$, as well as the angle α for the rhodium simulation. It is clear from the width of the $R_{M-O_{II}}$ peak that it cannot be derived from the convolution of the peaks corresponding to r_1 and r_2 distances, but rather from the participation of the angle α. A different way to explore this geometrical relation is to use eq 3, which allows the computation of $R_{MO_{II}}$ by applying the instantaneous value for any one of these geometrical parameters (r_1, r_2, or α) from a simulation snapshot and replacing the other two parameters by their average values in the simulation ($\bar{r}_1$, $\bar{r}_2$, $\bar{\alpha}$).

$$R_{MO_{II}}(r_1, r_2, \alpha) = \frac{r_1 \sin \alpha}{\cos\left(-\frac{\alpha}{2} + \arctan\left(\frac{r_1 - r_2}{r_1 + r_2}\cot\frac{\alpha}{2}\right)\right)} \quad (3)$$

This computed value can be compared with the current one for

(47) Bol, W.; Gerrits, G. J. A.; van Panthaleon van Eck, C. L. *J. Appl. Crystallogr.* **1970**, *3*, 486.
(48) Richens, D. T. *The chemistry of aqua ions;* Wiley: Chichester, 1997.

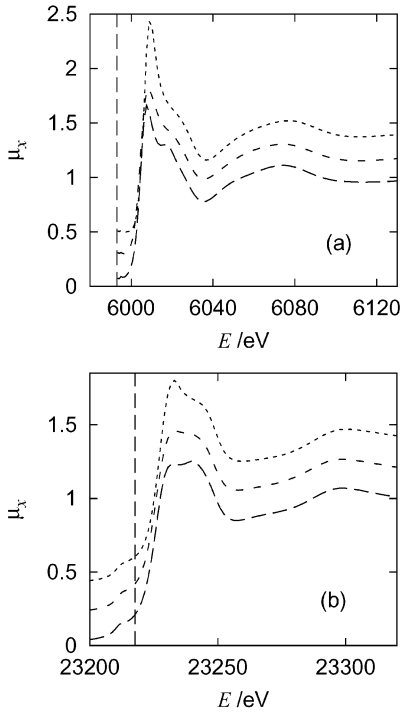

Figure 10. Calculated Cr (a) and Rh (b) K-edge XANES spectra averaged over spectra of the first hydration shell (dotted line), spectra of the complete potential calculation, but scattering contributions limited to the first hydration shell (dashed), and complete calculation (long-dashed). The dashed vertical line indicates the Fermi level of the calculated spectrum (for computational details, see text).

the considered snapshot. The correlation obtained is shown graphically for the rhodium simulation in Figure 9b−d. It is clear that the highest correlation is achieved with the angle, while there is a slight correlation with r_2. r_1 is negligibly correlated with $R_{MO_{II}}$, which means that its contribution to the DW factor of the ss2 path can be neglected. Similar results were obtained for the simulation of chromium. M, O_I, and O_{II} can be thought of as the vertexes of a deformable triangle where two sides, r_1 and r_2, are fixed in length, and the angle formed by these two sides (α) is the fluctuating parameter.

XANES Spectrum Features Associated with the Second Hydration Shell. The fully satisfactory match of the XANES spectra compelled us to study their dependence on the structure around the absorber atom. Figure 10a (Cr) and 10b (Rh) shows that coordination shells beyond the first one make an important contribution to the spectrum and are responsible for some of their features. The dotted lines correspond to the averages of spectra calculated for structures that consist of the absorber atom and its first hydration shell only. The structures were determined from the same snapshots used for the complete XANES calculation (long-dashed line). The dashed lines in Figure 10 were obtained with the clusters used in the complete calculation but considering as scatterers the first hydration shell atoms only. Thus, for these computed spectra, the photoelectron experiences the same potential as in the complete calculation. These results point out that the main effect of the second shell is to act on the modeling of the potential (dashed vs dotted lines) and thus on the mean free path of the photoelectron. The effect of the FMS is noticeable (long-dashed vs dashed lines), although lower in amplitude than the effect due to the potential.

A direct comparison of the spectra from first-shell-only clusters and complete clusters in rhodium and chromium (upper and lower lines in Figure 10a,b) reveals that second hydration shell operates on the features of the XANES in the same sense for both cations, that is, increasing the relative intensity of the peak just after the main edge resonance. The increment in absorption in this region with respect to the averaged spectrum obtained from only the first shell is comparable in magnitude for both cations and gives the net effect of the second shell.

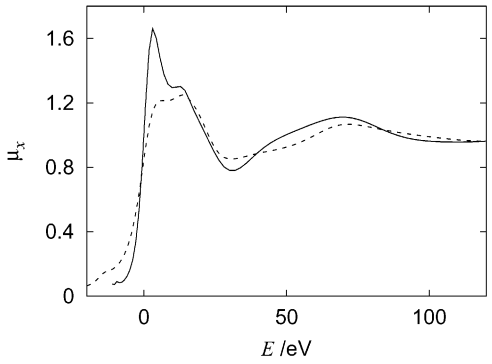

Figure 11. Calculated K-edge XANES spectra using Cr snapshots. Solid line is for Cr central atom, dashed for Rh.

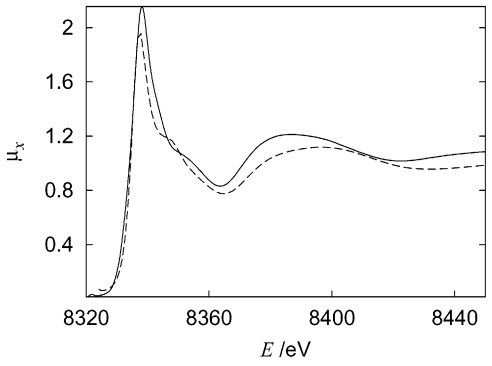

Figure 12. K-edge XANES spectra of Ni^{2+} in aqueous solution: experimental (solid line) and calculated (dashed). Atomic positions were taken from snapshots of Cr simulation and used for the calculation.

Figure 11 illustrates how the shape of the K-edge absorption spectrum depends on the atomic number considered. To eliminate differences in structure in this discussion, snapshots of the Cr^{3+} aqueous solution simulation were used for the calculation of both the chromium and rhodium spectra. In the latter case, the chromium atom was replaced by rhodium, and the K-edge spectra were computed. Both lines have been represented relative to the rising edge. For higher atomic numbers, lifetime broadening is increased, and spectra lose resolution. The absorption edge is less intense and broader. In the case of rhodium, the shoulder or second peak is more intense than in chromium. The quite reasonable reproduction of the rhodium XANES spectrum based on the chromium structures suggests that this procedure may be extended to other hexahydrated cations. It is applied to the case of Ni^{2+} in water, whose computed spectrum is shown in Figure 12, together with an experimental one. Nickel has an octahedral first hydration shell: the average $M-O_I$ distance is slightly larger than for the chromium hydrate (see Table 5) and the residence time of the water molecules in the first shell is lower,[16] but the structure of a chromium aqueous solution is a reasonable first approximation. The calculated XANES spectrum collects the main features of the experimental one, although the agreement is not as good as that found for the trivalent case of rhodium. This means that

the degree of transferability to other cations is affected by some uncertainty, which must be taken into account in order to draw conclusions from further analysis. Additional detailed comparisons between extrapolated results and those obtained from the proper cation studied must be undertaken to gain insight into this point. This kind of procedure, which implies a kind of "transmutation" of the absorber atom, is not redundant with the EXAFS results given in Table 5, but rather complementary. When methodology is appropriate, a given average structure and its associated fluctuations must produce computed XAS spectra whose comparison to the experimental ones reflects a consistent global spectroscopic answer.

Conclusions

EXAFS and XANES spectra of Cr^{3+} and Rh^{3+} aqueous solutions obtained by combining the structural information derived from MD simulations and quantum-mechanical calculations of XAS spectra agree fairly well with experimental spectra. The comparative analysis of experimental and simulated spectra shows that, for both chromium and rhodium, structural parameters of the second hydration shell can be determined accurately enough. Two points must be stressed. The first concerns the fact that two very similar hydration structures around two trivalent cations do not give such similar EXAFS nor XANES spectra. The second is related to the second hydration shell determination. The difficulty of determining its structure is due to the fact that it is a minor contribution to the EXAFS signal, hence the relevance of introducing independent structural information to help in the refined analysis of the XAS spectra.

Relationships between Debye−Waller factors applicable to other metal cations in octahedral environment were established. Using these relationships, the determination of structural parameters from an experimental EXAFS spectrum is possible with only a few assumptions (for example, an estimate of the experimental energy broadening of the system). The procedure here proposed was applied successfully to the case of Ni^{2+} in water. There are no fundamental reasons to believe that this methodology will not work when considering other geometrical arrangements of ion solvation (for changes both in the coordination number and in the coordination geometry). Two points have to be explored. First is the degree of transferability of the DW ratios, which will have to be heuristically determined. Second is the definition of correct intermolecular potential for other metal hydrated cations when the stability is not as high as in the case of the trivalent cations here examined. The basic problem lies in the degree of well-defined polyhedron which could be associated with the hydrate. This behavior must also affect the second hydration shell contribution, the influence of which on the XAS spectra will probably decrease with less-charged cations and the lability of the hydrate.

The XANES spectra are strongly influenced by the second hydration shell. This fact opens the door to the structural determination of some parameters by using numerical optimization procedures, as Benfatto et al. recently suggested.[49] It is not yet possible to deal with the whole quantitative structural information of the system, but a promising perspective may be envisaged. The combination of computer simulations and XANES may provide a powerful tool which would supply a global insight into the structure of the system. It is complementary to the EXAFS study in its ability to resolve angular properties of the system and represents an interesting alternative for radial information.

Acknowledgment. P.J.M. acknowledges financial support by the Deutsche Forschungsgemeinschaft. We acknowledge the Fundación Ramón Areces (XI Concurso Nacional) for financial support. J. M. Martínez is acknowledged for providing us with the parameters of his newly developed rhodium potential. We thank Stuart Ansell for his assistance during measurements at the ESRF synchrotron source (BM29) and the ESRF for beam time allocation (proposal CH-1192).

Supporting Information Available: Details about the Rh^{3+}−water intermolecular potentials, including the functional form and its coefficients; Figure S1, a comparison between the computed EXAFS spectra with and without including hydrogen atom scattering effects; an example of a typical FEFF (version 8.10) input file used to compute the XANES spectra; Table S1, third and fourth order cumulants of MD simulations of Cr^{3+} and Rh^{3+} in water; Figure S2, image of how the shape of the EXAFS spectrum is affected as a function of the number of snapshots selected and the timelength of the MD simulation for the case of the rhodium hydration (PDF). This material is available free of charge via the Internet at http://pubs.acs.org.

JA025729H

(49) Della Longa, S.; Arcovito, A.; Girasole, M.; Hasemann, J. L.; Benfatto, M. *Phys. Rev. Lett.* **2001**, *87*, 155501.